Damgaard-Møller, E., Krause, L., Lassen, H., Malaspina, L. A., Grabowsky, S., Bamberger, H., McGuire, J., Miras, H. N., Sproules, S. and Overgaard, J. (2020) Investigating complex magnetic anisotropy in a Co(II) molecular compound: a charge density and correlated ab initio electronic structure study. *Inorganic Chemistry*, 59(18), pp. 13190-13200.

(doi: 10.1021/acs.inorgchem.0c01489)

This is the Author Accepted Manuscript.

There may be differences between this version and the published version. You are advised to consult the publisher's version if you wish to cite from it.

https://eprints.gla.ac.uk/222386/

Deposited on: 19 August 2020

Enlighten – Research publications by members of the University of Glasgow
http://eprints.gla.ac.uk

Investigating complex magnetic anisotropy in a Co(II) molecular compound: A charge density and correlated ab initio electronic structure study

Emil Damgaard-Møller,[1] Lennard Krause,[1] Helene Lassen,[1] Lorraine A. Malaspina,[2] Simon Grabowsky,[3] Heiko Bamberger,[4] Jake McGuire,[5] Haralampos N. Miras,[5] Stephen Sproules[*5] and Jacob Overgaard*[*1]

[1] Department of Chemistry, Aarhus University, Langelandsgade 140, DK-8000 Aarhus C, DK.

[2] Department 2 – Biology/Chemistry, University of Bremen, Leobener Str. 3, 28359 Bremen, Germany

[3] Department of Chemistry and Biochemistry, University of Bern, Freiestrasse 3, 3012 Bern, Switzerland

[4] Institut für Physikalische Chemie, Universität Stuttgart, Pfaffenwaldring 55, D-70569 Stuttgart, Germany

[5] WestCHEM, School of Chemistry, University of Glasgow, Glasgow G12 8QQ, Glasgow, UK

Abstract

Understanding magnetic anisotropy and specifically how to tailor it is crucial in the search for high-temperature single-ion magnets. Herein, we investigate the magnetic anisotropy in a six-

coordinated cobalt(II) compound having a complex geometry and distinct tri-axial magnetic anisotropy from the perspective of the electronic structure, using electronic spectra, ab initio calculations, and an experimental charge density, of which the latter two provides insight into the d-orbital splitting. The analysis showed that the d-orbital splitting satisfactorily predicted the complex tri-axial magnetic anisotropy exhibited by the compound. Furthermore, a novel method to directly compare the ab initio results and the d-orbital populations obtained from the experimental charge density was developed, while a topological analysis of the density provided insights into the metal-ligand bonding. This work thus further establishes the validity of using d-orbitals for predicting magnetic anisotropy in transition metal compounds while also pointing out the need for a more frequent usage of the term tri-axial anisotropy in the field of single-molecule magnetism.

Introduction

Distorted tetrahedral cobalt(II) complexes represent a known class of single-ion magnets (SIMs) that exhibit slow relaxation of the magnetization in the absence of an external field.[1] For a transition metal complex to show SIM behavior, it must display zero-field splitting (ZFS), which, in the case of a molecule without first-order orbital momentum, can be quantified by two parameters, an axial ZFS parameter, D, and a rhombic ZFS parameter, E.[2] Optimal SIM properties are obtained with a significantly negative axial ZFS parameter, in combination with a small rhombic component, as a negative axial component describes a stabilization of the most magnetic ground state, while a non-zero value of E quantifies the effect of mixing of states with $\Delta M_S = \pm 2$, thereby creating rhombic anisotropy (*i.e.* anisotropy that is neither easy-axis nor easy-plane; in this work we use the term tri-axial anisotropy for such systems). Kramers ions (*i.e.* ions with half-integer spin) are often chosen in the search for new SIMs, as quantum tunneling of the

magnetization (QTM) in zero magnetic field is (when neglecting hyperfine coupling, dipole interactions, etc.) formally forbidden. As a consequence, all such complexes should exhibit SIM behavior, regardless of the sign and size of the ZFS parameters, and some complexes showing slow magnetic relaxation under applied field with a positive axial ZFS parameter have also been reported.[3-5] Such cases are, however, scarce and only compounds with a negative *D* parameter have been observed to show slow relaxation at zero field, emphasizing the importance of the sign of *D* and a minute *E* parameter, even for Kramers type complexes.

The first transition metal-based SIM to operate at zero field was $(PPh_4)_2[Co(SPh)_4]$, which possesses pseudo S_4 or D_{2d} symmetry with $D \sim -50$ cm^{-1} and a negligible *E* parameter.[1, 6] The geometry of this molecule is most appropriately described as tetrahedral with significant compression of two opposite S–Co–S angles.[7, 8] In subsequent studies of the family of compounds $(PPh_4)_2[Co(EPh)_4]$ (where E = O, S, Se, Te),[9, 10] it was found that heavier donor atoms (i.e., softer ligand) lead to improved SIM properties. However, of higher importance is the spatial disposition of donor atoms around the central paramagnetic ion, and the tetragonal elongation of the coordination sphere in the solid state toward D_{2d} symmetry, as shown by several tetrahedral cobalt complexes with hard ligands.[11-14] Enforcing such geometrical distortion should thus improve the SIM properties of tetrahedral cobalt(II) complexes; an obvious approach to this is the use of adequately designed bidentate ligands.

The heterocycle *N*-methylimidazole-2-thione (ImT) readily coordinates to transition metal ions to form complexes with a tetrahedral MS_4 central core. Emerald-green $[Co(ImT)_4]^{2+}$ with either nitrate or perchlorate counterions[15, 16] is nearly identical to the tetrathioureacobalt(II) complex mentioned above,[17] and, similar to the latter, it is a functioning SIM.[18] Unlike thiourea, the ImT unit is readily incorporated into a monoanionic bidentate ligand by reacting two

equivalents with borohydride to give the bis(2-mercapto-1-methylimidazolyl)borate anion, $(Bm^{Me})^-$.[19] These *S,S′* ligands, identified as soft scorpionates,[20] are part of the broad family of multidentate ligands based on progenitor polypyrazolylborates developed by Trofimenko.[21, 22] Although possessing a MS_4-core, structural studies have revealed a substantial departure from the expected tetrahedral geometry brought about by the formation of two 3-center/2-electron M···H–B agostic interactions.[23] An example is the $[M(Bm^{Me})_2]$ (M = Zn, Cd, Hg) series, which exhibit two *cis*-orientated M···H interactions at distances ranging 2.47 – 3.09 Å that push the sulfur donor atoms into a seesaw topology.[24] This phenomenon has also been observed in Co complexes with related sulfur-donor ligands.[25-27]

The compound investigated here, $[Co(Bm^{Me})_2]$, see Figure 1, is of interest due to its complex magnetic anisotropy, and understanding this may lead to novel design criteria for new SIMs. The magnetic anisotropy is analyzed and discussed based on the ab initio ligand field theory (AILFT) orbitals obtained from *ab initio* calculations. These observations are corroborated by an experimental electron density (ED) analysis, which provides d-orbital populations that are used to validate the obtained AILFT orbitals. A novel quantitation analysis of the d-orbital populations from *ab initio* calculations, which includes the bonding interactions, has been developed, making a direct comparison between the *ab initio* calculation and the experimental ED possible. Furthermore, a topological analysis of the experimental ED is performed, revealing information about bonding interactions. In particular, the Co···H–B agostic interactions and their impact on the ligand field are interesting. In contrast to d^0 metal alkyl complexes,[28, 29] ED studies of M···H–B interactions are unprecedented in the literature.

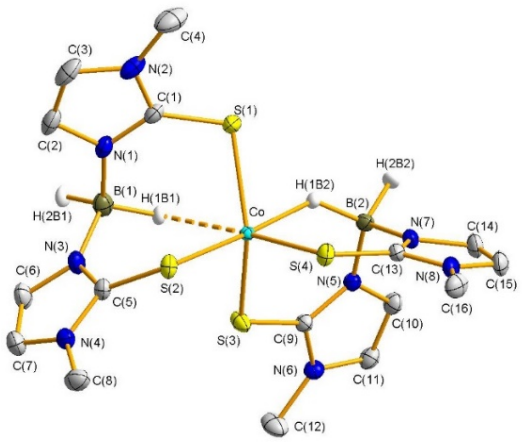

Figure 1. Thermal ellipsoid depiction of the structure of [Co(Bm^{Me})$_2$] showing atomic displacement parameters using 50% probability surfaces. All hydrogens except the four hydrogens on boron have been omitted for clarity. The longer Co···H(1B1) bond is shown as a dashed line.

Experimental Methods

The sodium salt of dihydrobis(2-mercapto-1-methylimidazolyl)borate anion, Na(Bm^{Me}), was prepared following the procedure of Alvarez *et al.*[24] All other reagents were used as received. Infrared spectra were collected using either a Shimadzu IRAffinity-1S or a Shimadzu FTIR 8400S spectrophotometer as neat powders. Electronic spectra were recorded from a Shimadzu UVA 3600 spectrophotometer (range 300 – 2500 nm). Solution magnetic susceptibilities were determined by the Evans method.[30] Electrospray ionization (ESI) mass spectra were obtained on a Bruker microTOF-Q mass spectrometer.

Synthesis of [Co(Bm^{Me})$_2$]. A stirred solution of $CoCl_2 \cdot 6H_2O$ (0.090 mg; 0.378 mmol) in H_2O (15 mL) was treated dropwise with a 10 mL aqueous solution of Na(Bm^{Me}) (0.200 g; 0.763 mmol) added over 10 min. A dark khaki brown precipitate rapidly evolved, which was collected by vacuum filtration. The solids were reconstituted in CH_2Cl_2 and layered with hexanes to produce a dark brown microcrystalline solid, which was filtered and dried in air. Yield: 0.134 g (66%). IR

(cm^{-1}): 3163 w, 3130 w, ν(BH) 2366 m, 2329 w, ν(CN) 1556 m, 1456 s, 1420 s, 1379 s, 1323 m, ν(C=S) 1188 s, 1171 s, 1119 s, 1080 s, 1035 m, 958 w, 864 w, 829 w, 718 s, 698 s, 675 s, 515 s. Electronic spectrum (CH_2Cl_2; λ_{max} / nm (ε / M^{-1} cm^{-1})): 1561 (140), 1097 (30), 807 (sh, ~40), 678 (460), 562 (960), 542 (sh, ~900), 442 (sh, ~6600), 412 (12,600), 375 (sh, ~ 5600). ESI mass spectrum: *m*/*z* 536 $[M]^+$.

Magnetic measurements. Magnetic measurements were performed in the temperature range from 1.8 to 300 K with a Quantum Design MPMS-XL-5 SQUID magnetometer equipped with a 7 T magnet. The powdered sample was contained in a gelatin capsule and fixed in a non-magnetic sample holder. Data were corrected for underlying diamagnetism using tabulated Pascal's constants.[31]

Single-Crystal X-ray Diffraction. Diffraction-quality green single crystals of $[Co(Bm^{Me})_2]$ were grown by diffusion of hexanes into a saturated dichloromethane solution of the complex. A single crystal was measured at BL02B1 on SPring-8 with a wavelength of 0.2480 Å and a temperature of 100 K. The crystal quality was found to deteriorate upon cooling to temperatures below 50 K, and for that reason lower temperatures were not used. The scattering was collected with a Dectris PILATUS3 X CdTe 1M detector, which we have recently found to provide extremely high quality charge density data.[32] Three ω-scans were performed using 1.0 sec/frame and a frame width of 0.5°. As ω was in the range from 0° to 180°, a total of 360 images was obtained for each data set. For all data sets, the 2θ-angle was fixed at 0°, while χ was set to 0°, 20° and 40°, respectively, to ensure optimal coverage of reciprocal space. An additional measurement was made with 4.0 sec/frame and frame width of 0.5°, ω in the range from 0° to 180°, 2θ = 0° and χ = 0° to obtain a data set with better statistics of high resolution data.

The measured images were converted to a set of integrated and scaled intensities using Apex3. The combination of a relatively high data collection temperature of 100 K and the weak scattering of the crystal led to a resolution limit of 0.50 Å. SADABS[33] was used to correct for absorption and other random errors by comparison of equivalent reflections and fitting of frame scale factors. Finally, SORTAV[34] was used to provide merged intensities and properly associated error estimates. The structure was solved using SHELXT[35] and refined using SHELXL,[36] both within the Olex2 program package.[37] The ED was modeled using XD2016,[38] which is based on the Hansen-Coppens multipole formalism, in which the atomic density for each atom is expanded into three terms: an unperturbed spherical core, a spherical valence term that allows refinement of valence population parameters and thus electron transfer between atoms, and finally an aspherical term that includes a set of refinable multipole population parameters that re-distribute the spherically organized valence electrons of a given atom using spherical harmonic angular functions.[39] We have recently reviewed the use of the ED approach in molecular magnetism.[40] The multipole model uses a local coordinate system defined as *z*: Co–S(4) and *x*: Co–S(2). All C–H distances were fixed at mean bond length values obtained from tabulated neutron diffraction data.[41] The tabulated mean bond length value for the B–H bond is insufficient for this compound, as one could expect the bond to be elongated due to the interaction with the central cobalt ion. Instead, the atomic coordinates for the boron-bonded hydrogen atoms were refined freely. Anisotropic thermal parameters for the hydrogen atoms were obtained from SHADE.[42] Since it is not a standard procedure to freely refine hydrogen atom parameters in multipole modeling, and since neutron diffraction data are not available, we resorted to a Hirshfeld Atom Refinement (HAR)[43, 44] as an independent second model to investigate the hydrogen atom positions in the Co vicinity. HAR is known to produce X-H bond distances with the same accuracy and precision from X-ray

diffraction data as those derived from neutron diffraction, including B-H and Fe-H bonds.[45] This is the first example of HAR for Co and the first open-shell HAR. HAR was carried out with the interface lamaGOET,[46] interfacing Gaussian09[47] for the wavefunction calculation at UB3LYP/cc-pVTZ level of theory and Tonto[48] for the non-spherical atomic form factor calculation and structural refinement. All positional and ADP parameters were refined freely, except for the methyl hydrogen atoms that were refined isotropically. To estimate how reliable the X-H HAR-refined bond distances are in this case, we averaged the results for all C-H bonds and compared to averaged results from neutron-diffraction esperiments (1.099(9)Å for methyl groups and 1.082(13)Å for $C{=}C_{sp2}$-H bonds).[49] From HAR, the results are 1.085(13)Å and 1.089(7)Å with maximum outliers as big as 0.05Å. This means that the results are accurate, but the standard uncertainty associated with the B-H bonds is probably higher than the values obtained from the variance-covariance matrix reported in the main part.

Theoretical calculations. All calculations described in this section were performed with the electronic structure program ORCA.[50, 51] Geometry optimizations were carried out using the BP86 functional[52, 53] in both the gas phase and in a dielectric continuum with acetonitrile as solvent to examine the stability of the molecular structure in solution.[54] A segmented all-electron relativistic contracted basis set of triple-ζ quality (def2-TZVP)[55-57] was used for all atoms with Grimme's dispersion correction D3.[58, 59] A scalar relativistic correction was applied using the zeroth-order regular approximation (ZORA) method[60-62] as implemented by van Wüllen.[63] An auxiliary basis set was used to expand the electron density in the calculations in conjunction with the resolution of identity approximation.[64] Spin Hamiltonian parameters and absorption spectra were computed on crystallographic coordinates using state-averaged complete active space self-consistent field (SA-CASSCF).[65-67] The missing dynamic correlations were recovered by *N*-

electron valence perturbation theory to the second order (NEVPT2).[68-71] The active space was chosen to contain seven electrons in five orbitals. All states arising from the d^7 configuration (10 quartets and 40 doublets) were included. The spin-orbit coupling (SOC) was treated using the mean-field (SOMF) approximation.[72] The effective Hamiltonian approach was used to compute SH parameters.[73, 74] An ab initio ligand field theory (AILFT) calculation[75, 76] was used to yield both a description of the d-orbitals and of the ligand field. The coordinate system was obtained from a visualization of the AILFT orbitals and subsequent assignment of the most appropriate orbitals. The coordinate system was chosen such that the z-axis was along the lobe of d_{z^2} and x,y were along the lobes of $d_{x^2-y^2}$, and a new *ab initio* calculation was subsequently performed with this coordinate system. The coordinate system corresponds to *z*: Co–S(4), *x*: Co–S(2) where x is made perpendicular to the z axis, and y is determined by the cross-product of z and x. Note that this is the exact same coordinate system that is used in the charge density model and therefore enables a direct comparison between the two.

Results and Discussion

Synthesis and Characterization. The stoichiometric addition of $Na(Bm^{Me})$ to a Co(II) salt produces $[Co(Bm^{Me})_2]$ in high yield. The infrared (IR) spectrum exhibits the four characteristic bands at 1188, 1080, 718 and 515 cm^{-1} of the thioamide unit N–C=S of the imidazole-2-thione.[77] In addition, there are two bands at 2366 and 2329 cm^{-1} assigned as ν(B–H) stretches from the $(Bm^{Me})^-$ ligand, as seen in related complexes with group 12 metals.[24] The lower energy peak is ascribed to the M···H–B repeatedly encountered in solid state structures of complexes with dihydroborate ligands,[19, 24, 25, 78, 79] however, the number and intensity of these IR features can vary. The electronic spectrum of $[Co(Bm^{Me})_2]$ recorded in either MeCN or CH_2Cl_2 showed three low-energy ligand field (LF) transitions at 1561, 1097, and 807 nm. Two weak ligand-to-metal charge

transfer (LMCT) bands are found at 607 and 562 nm, from which the compound derives its brown color in solution. The $S = {}^3/_2$ spin ground state for a high-spin Co(II) d^7 central ion was confirmed by a solution magnetic moment of 4.2 μ_B.

Structural characterization. The solid state structure of $[Co(Bm^{Me})_2]$ has been determined by single-crystal X-ray diffraction. Salient bond distances and angles are listed in Table 1. The complex comprises a central Co ion with four sulfur atoms from the two bidentate $(Bm^{Me})^-$ ligands (Fig. 2). The first coordination sphere bond distances are 2.3499(3), 2.3265(3), and 2.3386(3) Å for Co–S(1), Co–S(3) and Co–S(4), respectively, with a longer bond of 2.4144(1) Å for Co– S(2), which matches the distances reported in other complexes with imidazole-2-thione ligands.[15, 16, 26, 27] The CoS_4 core is highly distorted from a tetrahedral geometry with the coordination sphere supplemented by two adjacent Co···H–B agostic interactions of varying magnitude. The departure from tetrahedral geometry is evidenced by the S–Co–S angles that range from 89.81(1)° to 139.69(1)°, where the latter is considerably larger than found in the $[M(Bm^{Me})_2]$ (M = Zn, Cd, Hg) series.[24] The large S(1)–Co–S(3) opening allows for a hydride from each of the BH_2 groups to interact with the Co ion, at distances of 2.44(1) Å and 1.95(1) Å for H(1B1) and H(1B2), respectively. One explanation for the longer Co–S(2) bond distance is the presence of H(1B2) in the *trans*-position (the S(2)–Co–H(1B2) angle is 174.1(4)°). The two Co···H–B contacts are shorter than those identified in $[Co(Tm^{Me})_2]$ (Tm^{Me} = hydrotris(2-mercapto-1-methylimidazolyl)borate) at 2.27 and 2.34 Å,[25] $[Co(Btt^{Me})_2]$ (Btt^{Me} = dihydrobis(1-methyl-5-thiotetrazolyl)borate) at 2.32 and 2.58 Å,[80] $[Co(L)_2]$ (L = hydro[bis(3-*p*-tolyl-2-thioimidazol-1-yl)-(3-phenyl-5-methylpyrazol-1yl)]borate) at 2.52 and 3.91 Å,[27] and the $[M(Bm^{Me})_2]$ (M = Zn, Cd, Hg) series.[24] Only one other compound, $[Co(Bp^{tBu,iPr})_2]$ ($Bp^{tBu,iPr}$ = dihydrobis(3-*tert*-butyl-5-isopropylpyrazol-1-yl)borate) has similarly short contacts, with its distorted octahedral

coordination sphere completed by *trans* Co···H–B interactions at 1.94 Å.[81] The HAR results confirm the Co…H-B coordination mode with Co…H distances of 2.525(13) and 1.959(12)Å. The shorter B-H(1B1) distance is 1.174(13)Å, which agrees with earlier HAR-refined B-H distances for diborane of 1.170(7)/1.168(6) Å.[45] This also means that the elongated B-H(1B2) distance of 1.246(12) Å represents a significant activation of this B-H bond.

Table 1. Salient bond distances (Å) and angles (°) in $[Co(Bm^{Me})_2]$.

Co–S(1)	2.3499(3)	Co–S(2)	2.4144(1)
Co–S(3)	2.3265(3)	Co–S(4)	2.3386(3)
Co–H(1B1)	2.44(1)	Co–H(1B2)	1.95(1)
S(1)–Co–S(2)	102.72(1)	S(1)–Co–S(3)	139.69(1)
S(1)–Co–S(4)	108.73(1)	S(2)–Co–S(3)	96.26(1)
S(2)–Co–S(4)	89.81(1)	S(3)–Co–S(4)	106.53(1)
S(1)–Co–H(1B1)	73.0(3)	S(1)–Co–H(1B2)	73.6(5)
S(2)–Co–H(1B1)	85.4(4)	S(2)–Co–H(1B2)	174.1(4)
S(3)–Co–H(1B1)	73.5(3)	S(3)–Co–H(1B2)	89.4(4)
S(4)–Co–H(1B1)	175.2(4)	S(4)–Co–H(1B2)	87.0(4)
H(1B1)–Co–H(1B2)	97.8(6)		

Continuous shape measurement (CShM)[82] analysis emphasizes the strongly distorted molecular geometry of $[Co(Bm^{Me})_2]$. Assuming a five-coordinated complex, where the longer Co···H interaction is ignored, the geometry with the lowest CShM value is trigonal bipyramidal (2.5), while if both Co···H–B interactions are ignored, the lowest value (1.8) is obtained for an axially vacant trigonal bipyramid geometry (Table 2). To put these values into perspective, the CoS_4 moiety alone gives a CShM value of 2.4 for tetrahedral geometry. These variations in CShM values show that there is no clearcut best choice for the molecular coordination geometry.

Table 2. Continuous shape measures for selected geometries.

Geometry	CN[a]	CShM
Tetrahedral	4	2.4
Seesaw	4	3.9
Axial vacant trigonal bipyramid	4	1.8
Trigonal bipyramid	5	2.5
Square pyramidal	5	4.1
Octahedral	6	4.0
Trigonal prism	6	10.3

[a] CN = coordination number.

Theoretical calculations.

DFT calculations. To examine the integrity of the molecular structure in solution, a geometry optimization starting from crystal structure coordinates was undertaken using DFT calculations employing the BP86 functional with and without a solvent continuum. In both cases, the optimized structure preserved the Co···H interactions at 1.96 and 3.01 Å (Fig. S2). The average Co–S bond distance and S–Co–S angle of 2.321 Å and 108.3°, respectively, match the solid state crystal structure (Table S5). In contrast, starting from a tetrahedral CoS_4 geometry, and in the absence of a solvent continuum, the optimization resulted in a more tetrahedral geometry than observed experimentally, with a shorter average Co–S distance at 2.298 Å, a more obtuse average S–Co–S bond angle of 112° and the nearest hydrogen atom being 2.79 Å from the Co ion (Fig. S3). Given the relatively minor change between crystallographic and geometry optimized structures, the electronic structure and properties of $[Co(Bm^{Me})_2]$ were calculated using the geometry obtained from the crystal structure (see next section). This assessment is supported by electronic spectroscopy recorded on separate dichloromethane and acetonitrile solutions of the

complex at ambient temperature. The spectra are superimposable despite the variation in solvent polarity, although there is a distinct brown color compared to the dark green color of the single crystals (vide supra). The color variation is attributed to the removal of lattice packing effects that modify the energy of ligand-to-metal charge transfer (LMCT) bands from the soft sulfur donor atoms. In contrast, polycrystalline salts of $[Co(ImT)_4]^{2+}$ are blue-green in the solid state but produce a lavender-colored solution in dichloromethane and pale pink in acetonitrile. This demonstrates a change in the first coordination sphere in solution that sees the addition of trace moisture and/or ligating solvent like MeCN producing an octahedral Co(II) complex.[83] The Co···H–B agostic interactions in $[Co(Bm^{Me})_2]$ persist in solution and prevent solvent coordination.

Ab initio calculations. The electronic structure of $[Co(Bm^{Me})_2]$ was calculated using the state-averaged complete active space self-consistent field (SA-CASSCF) method with *N*-electron valence second-order perturbation theory (NEVPT2). The CAS(7,5) calculation describes the seven valence electrons in the five d-orbitals of the Co(II) ion, and the 10 quartet and 40 doublet states were computed. The isolated d^7 ion possesses a ^4F ground term and a ^4P excited term destabilized by 15*B*, where *B* is the Racah parameter that represents interelectronic repulsion. The lowest doublet term, ^2G, resides *B* above ^4P. In an octahedral ligand field, which is one possible interpretation of the molecular structure of $[Co(Bm^{Me})_2]$, the ^4F ground term is split into $^4T_{1g}$, $^4T_{2g,}$ and $^4A_{2g}$ while the ^4P is associated with a $^4T_{1g}$ only. Lowering of the symmetry to C_{4v}, and therefore describing the ligand field of $[Co(Bm^{Me})_2]$ as six-coordinate with approximately tetragonal elongation along H(1B2)–Co–S(2), results in the further splitting of the triply degenerate states: $^4T_{1g}$ into ^4E and $^4A_2$, and $^4T_{2g}$ into ^4E and $^4B_2$.[84] A $^4B_2$ state emerges from symmetry reduction of the $^4A_{2g}$ term from parent octahedral symmetry (Figure S5).

The computed d-orbital splitting for the Co(II) ion shows a pseudo-tetragonal ligand field with the d_{xz} and d_{xy} orbitals nearly degenerate and stabilized relative to d_{yz}, d_{z^2} and $d_{x^2-y^2}$ orbitals (Fig. 2). These orbitals are assigned as E, B_2, B_1, and A_1 in pseudo C_{4v} point symmetry. The electronic absorption spectrum of [Co(Bm^{Me})$_2$] is characterized by three LF bands at 6400, 9000, and 13 200 cm^{-1}, as evidenced by the small extinction coefficients (Fig. 3). These spin-allowed transitions take place from the $^4A_2$ ground state to each of the four excited states derived from the $^4T_{1g}$, $^4T_{2g}$ and $^4A_{2g}$ parent terms in O_h symmetry.

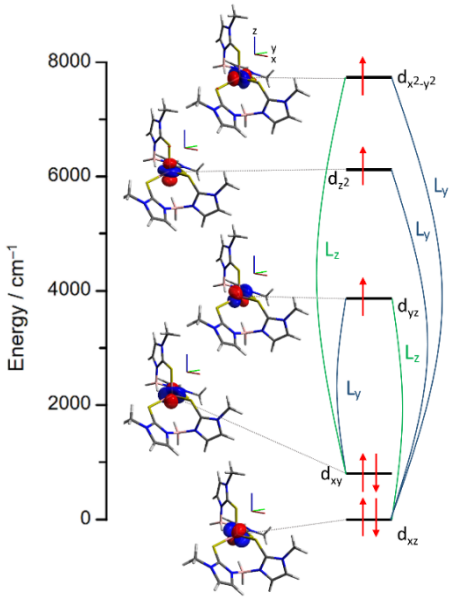

Figure 2. Energy of d-orbitals for [Co(Bm^{Me})$_2$] obtained from AILFT analysis of the SA-CASSCF(7,5) calculation. Coupling only occurs between doubly occupied orbitals and singly occupied orbitals, and the operator responsible for the coupling of two orbitals is shown, green line: L_z, blue line: L_y.

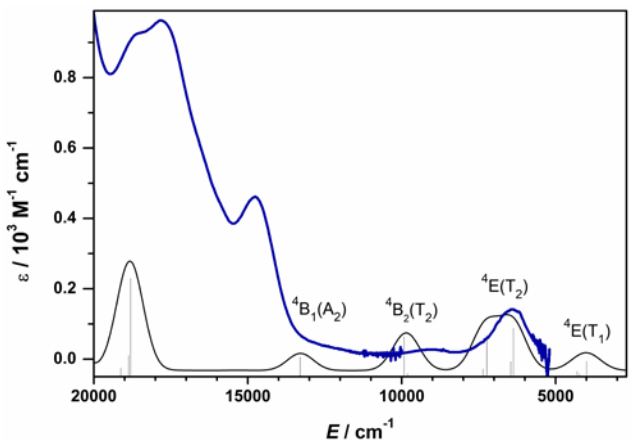

Figure 3. Comparison of the experimental (blue) and calculated (black) electronic absorption spectrum for $[Co(Bm^{Me})_2]$. The theoretical spectrum is produced from SOC-CASSCF(7,5)/NEVPT2 calculation with a Gaussian line broadening of 1000 cm^{-1}. Vertical lines represent individual transitions with the four lowest energy bands assigned.

The lowest energy $^4A_2 \rightarrow {}^4E$ is calculated at 3984 and 4183 cm^{-1} and resides outside the detection window of the spectrometer (Table S6). The $^4A_2 \rightarrow {}^4E(T_2)$ matches well to the lowest energy band in the experimental spectrum. The calculated peak is broadened by the lower symmetry in $[Co(Bm^{Me})_2]$ compared with an idealized pseudo-tetragonal structure. The remaining two LF transitions are calculated at 9860 cm^{-1} for $^4A_2 \rightarrow {}^4B_2(T_2)$ and 13 290 cm^{-1} for $^4A_2 \rightarrow {}^4B_1(A_2)$, and are an excellent match to the experimental energies of 9000 and 13 200 cm^{-1}, respectively. The excitations to the quartet states derived from the ^4P excited term, as well as possible spin-forbidden transitions to doublets states that derive from the ^2G term, which gain intensity from the lowering of symmetry, are all buried beneath the suite of LMCT bands starting at 15 000 cm^{-1}. Overall, the calculated LF transitions are in excellent agreement with the experimental data and confirms the solid state structure to be largely unchanged in solution.

The *ab initio* magnetic anisotropy parameters calculated from the effective spin-Hamiltonian $\widehat{H} = \widehat{\boldsymbol{S}} \cdot \overline{\overline{D}} \cdot \widehat{\boldsymbol{S}}$ for [Co(Bm^{Me})$_2$] are D = 19.1 cm^{-1} and E/D = 0.29, indicating a very rhombic – nearly perfectly tri-axial – magnetic anisotropy, which is only rarely observed and commented on in the literature.[85, 86] These values are in good agreement with the experimental values of D = 16.4 cm^{-1} and E/D = 0.19, as obtained from fits to magnetic susceptibility and magnetization curves (Figures S6 and S7). Tri-axial anisotropy implies a $g_x < g_y < g_z$ relationship, in contrast to easy-plane and easy-axis anisotropy, which is characterized by $g_z < g_x = g_y$ and $g_x = g_y < g_z$, respectively. Up to now, the overwhelming majority of research on molecular magnets has focused exclusively on the sign of D to determine whether a compound exhibits easy-plane or easy-axis anisotropy, while the magnitude of E is often reported, but rarely commented on. We thus use this opportunity to discuss the importance of the rhombic ZFS parameter, E.[87,88,89]

A value of $E/D = {}^1/_3$ describes a situation with perfect tri-axial magnetic anisotropy, and in that particular situation, tiny distortions to the molecular geometry can transform the D-value from very positive to very negative, rendering the concept of easy-axis and easy-plane anisotropy moot. We have illustrated this effect in Fig. 4, which has been constructed with one fixed eigenvalue of the D-tensor (20 cm^{-1}), while the second eigenvalue varies from -10 cm^{-1} to +20 cm^{-1} along the abscissa (the third eigenvalue is then inherently fixed from the traceless property of the tensor, see ESI for further details). Fig. 4 shows an abrupt and discontinuous shift from positive to negative D at exactly the point where $E/D = {}^1/_3$. This sudden change in D is accompanied by a change of axes, as seen here in the [Co(Bm^{Me})$_2$] complex, where D is associated with the molecular x-axis if it is positive and with the molecular y-axis if it is negative. This is a direct result of the requirement that $|D| \geq 3E \geq 0$. In Fig. 4, we have separated the easy-plane | tri-axial | easy-axis regimes by dashed vertical lines, although there is no strict physical justification for this. It serves

mostly to emphasize that the characterization of magnetic anisotropy is not a simple choice of one or the other type.

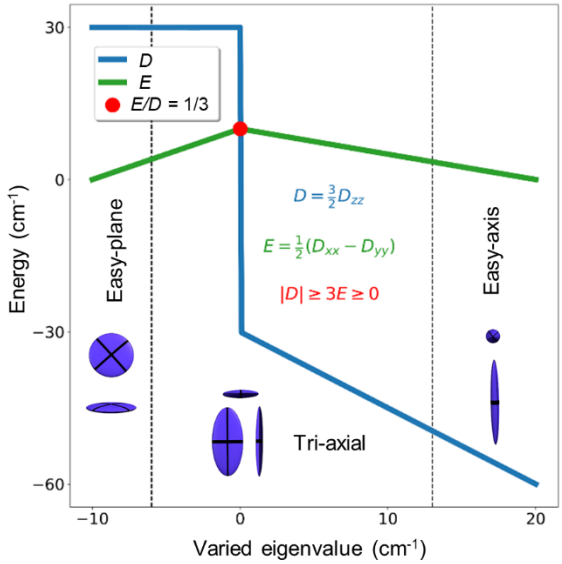

Figure 4. Calculated *D* and *E* in the case of one fixed eigenvalue of the *D*-tensor (20 cm^{-1}) and varied second eigenvalue (*x*-axis of the graph). Susceptibility ellipsoids, which represent the type of anisotropy, are visualized in the respective regimes (left: easy-plane, middle: tri-axial, right: easy-axis).

We now turn to the rationalization of the magnetic anisotropy from the calculated d-orbital splitting (Fig. 2). The coordinate system defining these orbitals was chosen such that the AILFT orbitals represent the purest d-orbital description (see the experimental section). This coordinate system thus gave pure d_{z^2} and $d_{x^2-y^2}$ orbitals, while the three remaining orbitals display a slight mixing (see ESI for further details). One of the main advantages of using the d-orbitals and their energies for predicting the sign and size of the magnetic anisotropy is the chemically intuitive toolbox it provides. Although the approach might not be accurate or even physically unassailable, it has proven effective in predicting the magnetic anisotropy in several complexes.[90, 91] However, the method has hitherto primarily been confined to the extremes of easy-axis or easy-plane

magnetic anisotropy, while it has rarely been applied to a description of such severe tri-axiality as exhibited by [Co(Bm^{Me})$_2$].[92] Now, to proceed, we use the assumption that the d-orbitals are pure, which forces the *D*-tensor to be diagonal (for details, see the ESI). To quantify the anisotropy, we are therefore left with the task of evaluating the possible couplings between the doubly occupied and singly occupied d-orbitals through the different L_u ($u = x, y, z$) operators. If two d-orbitals are coupled via a given operator L_u, this contributes to making the direction "*u*" easy to magnetize (*i.e.*, contributes negatively to D_{uu}), and the interaction strength scales with the inverse of the energy difference between the two coupled orbitals.[2] Thus, if one L_u operator dominates, easy-axis anisotropy is observed; if two L_u operators dominate, easy-plane anisotropy is observed, while if all three L_u operators contribute equally, the magnetism is isotropic.

In [Co(Bm^{Me})$_2$], the d_{xy} orbital is coupled with the d_{yz} and $d_{x^2-y^2}$ orbitals through the L_y and L_z operators, respectively, while the d_{xz} orbital is coupled with d_{yz}, d_{z^2}, and $d_{x^2-y^2}$ through L_z, L_y, and L_y, respectively (Fig. 4). Combining this knowledge with the calculated d-orbital energies, we conclude that the most easy axis is along the *y*-direction, since L_y is responsible for three couplings, and (most importantly) is the operator associated with the smallest energy difference (coupling of d_{xy} and d_{yz}). Similarly, there will be an intermediate axis along the *z*-direction, smaller in magnitude than along the *y*-direction. Lastly, the *x*-axis must be a hard axis, since no orbitals are coupled through the L_x operator. Thus, the analysis predicts that the anisotropy increases in the following way: $x < z < y$ (see ESI for further details).

The calculated eigenvalues and eigenvectors for the *D*- and *g*-tensors using the effective spin-Hamiltonian formalism are listed in Table 3. Since $g_x < g_y < g_z$ by definition, the above analysis predicts g_x to be along the *x*-direction in the molecule, g_y to be along the *z*-direction, and g_z to be along the *y*-direction, which is completely in accordance with the calculated eigenvectors

given in Table 3. Furthermore, since D (= $^3/_2\ D_{zz}$) is positive, D_{zz} must be along the hardest axis (x-axis), and as D_{yy} must be smaller than D_{xx} (given $E = (D_{xx}–D_{yy})/2 \geq 0$), D_{yy} is therefore along the y-axis, and D_{xx} along the z-axis, which is also consistent with Table 3. The simple approach of predicting the anisotropy using the d-orbitals and an analysis of the operators responsible for the coupling has thus proven to be valid even for highly distorted complexes as [Co(Bm^{Me})$_2$]. Furthermore, the fact that the eigenvectors of the D- and g-matrices are almost collinear with the axes of the chosen coordinate system for the orbitals (Table 3) justifies the assumption of pure d-orbitals (and diagonal D- and g-matrices).

Table 3. Calculated eigenvalues and eigenvectors for the effective spin-Hamiltonian parameters using a pseudo-spin S=3/2. Eigenvectors are given with the Cartesian axes chosen from the AILFT orbitals.

	Eigenvalue[a]	x	y	z
D_{xx}	-0.79	-0.05	-0.04	1.00
D_{yy}	-11.94	0.02	1.00	0.04
D_{zz}	12.73	1.00	-0.03	0.05
g_x	2.11	0.99	-0.03	0.16
g_y	2.23	-0.16	-0.02	0.99
g_z	2.35	0.02	1.00	0.02

Experimental electron density. As mentioned in the experimental section, the local coordinate system for cobalt used in the experimental electron density modeling of [Co(Bm^{Me})$_2$] has the z-axis defined along the Co–S(4) bond, the x-axis parallel to the Co–S(2) bond, with the y-axis being the normal vector to this xz-plane. This coordinate system is consistent with the

coordinate system chosen from the AILFT orbitals. Static model deformation density maps in the three planes (*xy*, *xz*, *yz*) formed by cobalt and atoms from the first coordination sphere are presented in Fig. 5. These deformation density maps represent the difference between the modeled experimental density and a fictitious spherical density (also known as the IAM density). The deformation density maps support the d-orbital splitting, $d_{xz} < d_{xy} < d_{yz}$, which is obtained from AILFT, as the maps clearly have the most positive contours in the *xz*-plane, slightly less in the *xy*-plane, and almost none in the *yz*-plane.

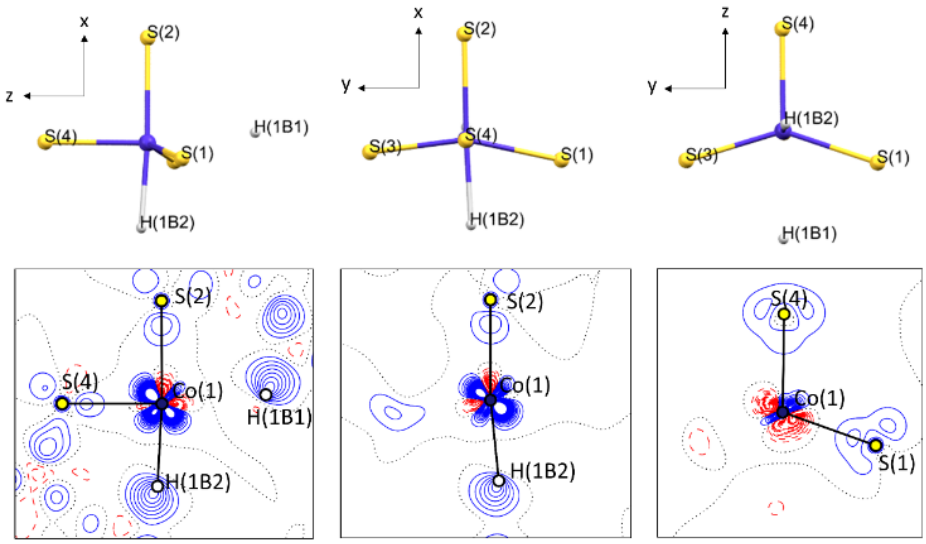

Figure 5. The three planes from the defined local coordinate system of the ED refinement (top) and the deformation density maps confirm the found energy ordering of the orbitals found from the *ab initio* calculation (bottom). The deformation density maps only show the atoms in-plane, which is why some figures seem to be missing atoms. Blue contours show positive values, red contours negative value, and the dotted black line shows the zero contour. Contour interval is 0.1 e $Å^{-3}$.

Experimental estimates of the d-orbital populations from the refined multipole model are obtained using the procedure developed by Holladay *et al.*,[93] and the results are summarized in

Table 4. It is clear that the two lower-lying orbitals are d_{xz} and d_{xy}, as they are nearly full (i.e., close to a population of 2 electrons), while the three other orbitals, d_{yz}, d_{z^2}, and $d_{x^2-y^2}$, are much closer to a population of 1 electron. If we assume that a large d-orbital population indicates a stabilization of that particular orbital, the obtained populations predict the relative d-orbital energies $d_{xz} < d_{xy} < d_{yz} < d_{z^2} < d_{x^2-y^2}$ which is consistent with the calculated d-orbital energy diagram seen in Fig. 2. In the most simple interpretation, we anticipate a distribution of the seven d-electrons on Co(II) as 2:2:1:1:1 in absolute numbers, or 28.8% and 14.4% in the doubly and singly occupied orbitals, respectively, as illustrated by the electron configuration in Fig. 2. However, such an approach ignores any bonding contributions involving the d-orbitals and the effect of spin-orbit coupling. We have therefore improved this estimate by exploiting the access to the CI-wavefunction from the *ab initio* calculation, together with the spin-orbit coupled wave functions. From these, we estimate the population of atom-centered d-orbitals from the CI + SOC calculation (Table 4), which already constitutes a significant improvement to the simple integral number population of the orbitals (for this procedure, see ESI). However, the inactive space should also be incorporated in the estimation of the d-orbital populations from an *ab initio* calculation, as some bonding molecular orbitals will contribute. This was done in the following way: if an inactive orbital had 0.5% contribution from, say d_{xz}, the contribution from that molecular orbital would be 0.005×2 electrons to the d_{xz} orbital. Summing up all contributions from the inactive orbitals, the d-orbital populations from the experimental ED and the *ab initio* calculation become closely matched (Table 4). Very recently some of us published results using the same approach to compare the experimentally determined d-orbital populations and the estimate from the CI + SOC *ab initio* wave function,[94] however, to the best of our knowledge, this is the first time experimental d-orbital

populations have been compared against *ab initio* calculations where the bonding interaction is included (see ESI for further details).

Table 4. Experimental and calculated d-orbital occupancy. In parentheses are given the percentage occupancy relative to the total occupancy of the d-orbitals.

	Experimental	Estimate from CI + SOC	Estimate including bonding contribution
$d_{x^2-y^2}$	1.15 (15.4)	1.00 (14.8)	1.30 (16.8)
d_{z^2}	1.26 (16.8)	1.00 (14.8)	1.26 (16.2)
d_{yz}	1.31 (17.5)	1.28 (18.9)	1.50 (19.3)
d_{xy}	1.70 (22.7)	1.65 (24.4)	1.79 (23.1)
d_{xz}	2.07 (27.6)	1.83 (27.1)	1.90 (24.5)
Total	7.48	6.76	7.76

Topological analysis. The chemical bonding in $[Co(Bm^{Me})_2]$ can be quantified by a topological analysis of the experimental ED (see Table 5). Based on the quantum theory of atoms in molecules (QTAIM),[95] this approach locates critical points (CPs) in the ED where the local gradient is zero, *i.e.*, minima, maxima, and saddle points in the continuous ED. Of the four possible types of CPs, those with one negative and two positive negative curvatures are denoted the bond critical points, BCPs. Evaluation of the topological properties at the BCPs has traditionally been used to characterize the nature of the interaction using the Laplacian of the ED ($\nabla^2\rho_{bcp}$), which is the sum of the eigenvalues of the Hessian matrix, i.e. the symmetrical 3x3 matrix consisting of the derivative of the ED with respect to the x,y,z directions. The eigenvalues of this matrix are the curvatures along the eigen-directions and are denoted $\lambda_{1\text{-}3}$, and the ellipticity (ε) is the difference from unity of the ratio of the two negative curvatures. This approach is very useful to distinguish

between covalent and ionic bonding, particularly between light atoms,[96] while it is less clear-cut for metal-ligand bonds. We find that the total energy density, H, at the BCPs is negative for all Co–S bonds, suggesting that there are substantial covalent contributions to these bonds. The analysis also clearly finds BCPs in the Co-H bonds, with significant values of ED at the BCP, thus confirming that cobalt is six-coordinate.

Table 5. Topological properties at selected BCP. The value of ρ_{BCP} is given in eÅ^{-3}, the Laplacian ($\nabla^2\rho_{BCP}$) in eÅ^{-5}, distances in Å, while the kinetic, potential, and total energy densities G, V and H, respectively, are given in Hartree au^{-3}.

Bond (1-2)	ρ_{BCP}	$\nabla^2\rho_{BCP}$	d	$d_{1\text{-}BCP}$	$d_{2\text{-}BCP}$	ε	G	H	V
Co–S(1)	0.448	3.618	2.3500	1.0860	1.2640	0.05	0.38	-0.51	-0.13
Co–S(2)	0.408	3.370	2.4145	1.1097	1.3048	0.05	0.34	-0.44	-0.10
Co–S(3)	0.468	3.913	2.3265	1.0795	1.2470	0.06	0.41	-0.55	-0.14
Co–S(4)	0.461	3.997	2.3386	1.0891	1.2496	0.06	0.41	-0.54	-0.13
Co–H(1B2)	0.255	2.156	1.9611	1.2429	0.7182	0.19	0.18	-0.22	-0.03
Co–H(1B1)	0.127	0.829	2.4570	1.4962	0.9608	0.11	0.06	-0.07	-0.01

Conclusions

The robust Co···H-B agostic interactions that appear in [Co(Bm^{Me})$_2$] and intrude into the coordination space and displace the sulfur donor atoms result in a molecular complex that exhibits both a complicated geometry, and a similarly complicated magnetic anisotropy. The comparison of the estimated anisotropy from the calculated AILFT scheme with the calculated effective spin-Hamiltonian parameters showed that such an analysis is fruitful even for geometrically and magnetically very complex systems.

Easy-axis magnetic anisotropy is frequently declared to arise from coupling of orbitals through the L_z operator (i.e., coupling of orbitals sharing the same $\pm m_l$ value).[17, 90, 97-99] While this is often true, it is not a strict requirement, as easy-axis anisotropy will arise from coupling through *any* L_u operator, as long as this one single operator is dominant, compared to the others. Based on an in-depth analysis of the magnetic anisotropy, we emphasize here the importance of *E* in the description of the anisotropy, and propose the term tri-axial anisotropy, as relying on the terms "easy-axis anisotropy" and "easy-plane anisotropy" determined entirely from the *sign* of *D* is often insufficient in describing the true anisotropy. Furthermore, low temperature synchrotron X-ray single-crystal diffraction data allowed the multipole modeling of the ED, from which d-orbital populations were extracted, very well aligned with the predicted occupancies from the obtained AILFT orbitals. Based on this description, we developed a model that enables a direct comparison between the multireference *ab initio* calculation and the experimentally derived d-orbital population and thereby reached a quantitative agreement.

ASSOCIATED CONTENT

Supporting Information.

The following files are available free of charge.

Details of X-ray data reduction, magnetic measurements and description of ab initio results.

(PDF)

AUTHOR INFORMATION

Corresponding Author

*jacobo@chem.au.dk; Stephen.sproules@glasgow.ac.uk

Author Contributions

The manuscript was written through contributions of all authors. All authors have given approval to the final version of the manuscript.

Funding Sources

Danish National Research Foundation; Villum Foundation.

ACKNOWLEDGMENTS

The authors gratefully acknowledge financial support from the Danish National Research Foundation (DNRF-93), the VILLUM FOUNDATION (12391), Danscatt, and DFG GR 4451/2-1. The synchrotron experiment was performed on beamline BL02B1 at SPring-8 with the approval of the Japan Synchrotron Radiation Research Institute as a Partner User (proposal no. 2018B0078). Affiliation with the Center for Integrated Materials Research (iMAT) at Aarhus University is gratefully acknowledged.

ABBREVIATIONS

REFERENCES

1. Zadrozny, J. M.; Long, J. R., Slow Magnetic Relaxation at Zero Field in the Tetrahedral Complex $[Co(SPh)_4]^{2-}$. *J. Am. Chem. Soc.* **2011,** *133*, 20732.
2. Boča, R., Zero-field splitting in metal complexes. *Coordination Chemistry Reviews* **2004,** *248* (9), 757-815.
3. Vallejo, J.; Castro, I.; Ruiz-Garcia, R.; Cano, J.; Julve, M.; Lloret, F.; De Munno, G.; Wernsdorfer, W.; Pardo, E., Field-Induced Slow Magnetic Relaxation in a Six-Coordinate Mononuclear Cobalt(II) Complex with a Positive Anisotropy. *J Am Chem Soc* **2012,** *134* (38), 15704-15707.

4. Zadrozny, J. M.; Liu, J. J.; Piro, N. A.; Chang, C. J.; Hill, S.; Long, J. R., Slow magnetic relaxation in a pseudotetrahedral cobalt(II) complex with easy-plane anisotropy. *Chem Commun* **2012,** *48* (33), 3927-3929.
5. Gómez-Coca, S.; Urtizberea, A.; Cremades, E.; Alonso, P. J.; Camón, A.; Ruiz, E.; Luis, F., Origin of slow magnetic relaxation in Kramers ions with non-uniaxial anisotropy. *Nature Communications* **2014,** *5* (1), 4300.
6. Suturina, E. A.; Nehrkorn, J.; Zadrozny, J. M.; Liu, J.; Atanasov, M.; Weyhermüller, T.; Maganas, D.; Hill, S.; Schnegg, A.; Bill, E.; Long, J. R.; Neese, F., Magneto-Structural Correlations in Pseudotetrahedral Forms of the $[Co(SPh)_4]^{2-}$ Complex Probed by Magnetometry, MCD Spectroscopy, Advanced EPR Techniques, and ab initio Electronic Structure Calculations. *Inorg. Chem.* **2017,** *56*, 3102-31118.
7. Swenson, D.; Baenziger, N. C.; Coucouvanis, D., Tetrahedral Mercaptide Complexes. Crystal and Molecular Structures of $[(C_6H_5)_4P]_2M(SC_6H_5)_4$ Zomplexes (M = Cadmium(II), Zinc(II), Nickel(II), Cobalt(II), and Manganese(II)). *J. Am. Chem. Soc.* **1978,** *100*, 6.
8. Maganas, D.; Sottini, S.; Kyritsis, P.; Groenen, E. J. J.; Neese, F., Theoretical Analysis of the Spin Hamiltonian Parameters in $Co^{(II)}S_4$ Complexes, Using Density Functional Theory and Correlated ab initio Methods. *Inorg. Chem.* **2011,** *50*, 8741-8754.
9. Suturina, E. A.; Maganas, D.; Bill, E.; Atanasov, M.; Neese, F., Magneto-Structural Correlations in a Series of Pseudotetrahedral $[Co^{II}(XR)_4]^{2-}$ Single Molecule Magnets: An ab initio Ligand Field Study. *Inorg. Chem.* **2015,** *54*, 9948-9961.
10. Zadrozny, J. M.; Telser, J.; Long, J. R., Slow magnetic relaxation in the tetrahedral cobalt(II) complexes [Co(EPh)4]2− (EO, S, Se). *Polyhedron* **2013,** *64* (0), 209-217.
11. Carl, E.; Demeshko, S.; Meyer, F.; Stalke, D., Triimidosulfonates as Acute Bite-Angle Chelates: Slow Relaxation of the Magnetization in Zero Field and Hysteresis Loop of a Co-II Complex. *Chem-Eur J* **2015,** *21* (28), 10109-10115.
12. Fataftah, M. S.; Zadrozny, J. M.; Rogers, D. M.; Freedman, D. E., A Mononuclear Transition Metal Single-Molecule Magnet in a Nuclear Spin-Free Ligand Environment. *Inorganic Chemistry* **2014,** *53* (19), 10716-10721.
13. Rechkemmer, Y.; Breitgoff, F. D.; van der Meer, M.; Atanasov, M.; Hakl, M.; Orlita, M.; Neugebauer, P.; Neese, F.; Sarkar, B.; van Slageren, J., A four-coordinate cobalt(II) single-ion magnet with coercivity and a very high energy barrier. *Nature Communications* **2016,** *7*, 10467.
14. Thiel, A. M.; Damgaard-Møller, E.; Overgaard, J., High-Pressure Crystallography as a Guide in the Design of Single-Molecule Magnets. *Inorganic Chemistry* **2020,** *59* (3), 1682-1691.
15. Raper, E. S.; Nowell, I. W., Coordination Compounds of 1-Methylimidazoline-2-(3H)-thione and Metal Nitrates [M(II) = Co, Zn and Cd]. A Spectroscopic, Thermal Analysis and X-ray Diffraction Study. *Inorg. Chim. Acta* **1980,** *43*, 165-172.
16. Raper, E. S.; Nowell, I. W., The Crystal Structure of Tetrakis[1-methylimidazoline-2(3*H*)-thione]cobalt(II) Diperchlorate. *Acta Crystallographica Section B-Structural Science* **1979,** *B35*, 1600-1603.
17. Vaidya, S.; Tewary, S.; Singh, S. K.; Langley, S. K.; Murray, K. S.; Lan, Y.; Wernsdorfer, W.; Rajaraman, G.; Shanmugam, M., What Controls the Sign and Magnitude of Magnetic Anisotropy in Tetrahedral Cobalt(II) Single-Ion Magnets? *Inorg. Chem.* **2016,** *55*, 9564-9578.
18. Sproules, S.; van Slageren, J., Manuscript in Preparation.

19. Kimblin, C.; Bridgewater, B. M.; Hascall, T.; Parkin, G., The Synthesis and Structural Characterization of Bis(mercaptoimidazolyl)hydroborato Complexes of Lithium, Thallium and Zinc. *J. Chem. Soc., Dalton Trans.* **2000**, 891.
20. Spicer, M. D.; Reglinski, J., Soft Scorpionate Ligands Based on Imidazole-2-thione Donors. *Eur. J. Inorg. Chem.* **2009**, 1553.
21. Trofimenko, S., *Scorpionates: The Coordination Chemistry of Polypyrazolylborate Ligands*. Imperial College Press: London, 1999.
22. Pettinari, C., *Scorpionates II: Chelating Borate Ligands*. Imperial College Press: London, 2008.
23. Zins, E.-L.; Silvi, B.; Alikhani, M. E., Activation of C-H and B-H Bonds through Agostic Bonding: An ELF/QTAIM Insight. *Phys. Chem. Chem. Phys.* **2015,** *17*, 9258.
24. Alvarez, H. M.; Tran, T. B.; Richter, M. A.; Alyounes, D. M.; Rabinovich, D.; Tanski, J. M.; Krawiec, M., Homoleptic Group 12 Metal Bis(mercaptoimidazolyl)borate Complexes $M(Bm^R)_2$ (M = Zn, Cd, Hg). *Inorg. Chem.* **2003,** *42*, 2149.
25. Baba, H.; Nakano, M., Magnetic Properties of Cobalt(II/III) Complexes with Sulfur-Scorpionate Ligands. *Polyhedron* **2011,** *30*, 3182.
26. Mihalcik, D. J.; White, J. L.; Tanski, J. M.; Zakharov, L. N.; Yap, G. P. A.; Incarvito, C. D.; Rheingold, A. L.; Rabinovich, D., Cobalt Tris(mercaptoimidazolyl)borate Complexes: Synthetic Studies and the Structure of the First Cobaltaboratrane. *Dalton Transactions* **2004,** *4* (10), 1626-1634.
27. Shu, M.-H.; Tu, C.-L.; Cui, J.; Sun, J., Syntheses and Crystal Structures of Cadmium(II) and Cobalt(II) Complexes with Hydro[bis(3-*p*-tolyl-2-thioimidazol-1-yl)-(3-phenyl-5-methylpyrazol-1-yl)] Borate. *Chin. J. Inorg. Chem.* **2006,** *22*, 1507-1510.
28. Scherer, W.; Meixner, P.; Barquera-Lozada, J. E.; Hauf, C.; Obenhuber, A.; Bruck, A.; Wolstenholme, D. J.; Ruhland, K.; Leusser, D.; Stalke, D., A unifying bonding concept for metal hydrosilane complexes. *Angew Chem Int Ed Engl* **2013,** *52* (23), 6092-6.
29. Scherer, W.; McGrady, G. S., Agostic interactions in d0 metal alkyl complexes. *Angew Chem Int Ed Engl* **2004,** *43* (14), 1782-806.
30. Sur, S. K., Measurement of Magnetic Susceptibility and Magnetic Moment of Paramagnetic Molecules in Solution by High-Field Fourier Transform NMR Spectroscopy. *J. Magn. Reson.* **1989,** *82*, 169-173.
31. Bain, G. A.; Berry, J. F., Diamagnetic corrections and Pascal's constants. *J Chem Educ* **2008,** *85* (4), 532-536.
32. Krause, L.; Tolborg, K.; Gronbech, T. B. E.; Sugimoto, K.; Iversen, B. B.; Overgaard, J., Accurate high-resolution single-crystal diffraction data from a Pilatus3 X CdTe detector. *J Appl Crystallogr* **2020,** *53*, 635-649.
33. Krause, L.; Herbst-Irmer, R.; Stalke, D., An Empirical Correction for the Influence of Low-Energy Contamination. *J. Appl. Crystallogr.* **2015,** *48*, 1907.
34. Blessing, R., Outlier Treatment in Data Merging. *J. Appl. Cryst.* **1997,** *30*, 421.
35. Sheldrick, G. M., SHELXT – Integrated Space-Group and Crystal-Structure Determination. *Acta Cryst.* **2015,** *A71*, 3.
36. Sheldrick, G. M., Crystal Structure Refinement with SHELXL. *Acta Cryst.* **2015,** *C71*, 3.
37. Dolomanov, O. V.; Bourhis, L. J.; Gildea, R. J.; Howard, J. A. K.; Puschmann, H., Olex2: A Complete Structure Solution, Refinement and Analysis Program. *J. Appl. Cryst.* **2009,** *42*, 339-341.

38. Lewis, K., Platforms for antibiotic discovery. *Nat Rev Drug Discov* **2013,** *12* (5), 371-387.
39. Hansen, N. K.; Coppens, P., Electron Population Analysis of Accurate Diffraction Data. 6. Testing Aspherical Atom Refinements on Small-Molecule Data Sets. *Acta Cryst. A* **1978,** *A34*, 909.
40. Damgaard-Moller, E.; Krause, L.; Overgaard, J., Experimental Charge Densities from Multipole Modeling: Moving into the Twenty-First Century. *Structure and Bonding* **2020**, in press.
41. Allen, F. H.; Kennard, O.; Watson, D. G.; Brammer, L.; Orpen, A. G.; Taylor, R., Tables of Bond Lengths Determined by X-ray and Neutron Diffraction. Part 1. Bond Lengths in Organic Compounds. *J. Chem. Soc., Perkin Trans. 2* **1987**, S1.
42. Munshi, P.; Madsen, A. O.; Spackman, M. A.; Larsen, S.; Destro, R., Estimated H-atom anisotropic displacement parameters: a comparison between different methods and with neutron diffraction results. *Acta Crystallogr A* **2008,** *64* (Pt 4), 465-75.
43. Jayatilaka, D.; Dittrich, B., X-ray structure refinement using aspherical atomic density functions obtained from quantum-mechanical calculations. *Acta Crystallographica Section A* **2008,** *64*, 383-393.
44. Capelli, S. C.; Burgi, H.-B.; Dittrich, B.; Grabowsky, S.; Jayatilaka, D., Hirshfeld atom refinement. *IUCrJ* **2014,** *1* (5), 361-379.
45. Woinska, M.; Grabowsky, S.; Dominiak, P. M.; Wozniak, K.; Jayatilaka, D., Hydrogen atoms can be located accurately and precisely by x-ray crystallography. *Sci Adv* **2016,** *2* (5).
46. Malaspina, L. A.; Genoni, A.; Grabowsky, S., lamaGOET: An Interface for Quantum Crystallography. *J Appl Crystallogr* **2020**, in revision.
47. Frisch, M. J.; Trucks, G. W.; Schlegel, H. B.; Scuseria, G. E.; Robb, M. A.; Cheeseman, J. R.; Scalmani, G.; Barone, V.; Mennucci, B.; Petersson, G. A.; Nakatsuji, H.; Caricato, M.; Li, X.; Hratchian, H. P.; Izmaylov, A. F.; Bloino, J.; Zheng, G.; Sonnenberg, J. L.; Hada, M.; Ehara, M.; Toyota, K.; Fukuda, R.; Hasegawa, J.; Ishida, M.; Nakajima, T.; Honda, Y.; Kitao, O.; Nakai, H.; Vreven, T.; Montgomery Jr, J. A.; Peralta, J. E.; Ogliaro, F.; Bearpark, M. J.; Heyd, J.; Brothers, E. N.; Kudin, K. N.; Staroverov, V. N.; Kobayashi, R.; Normand, J.; Raghavachari, K.; Rendell, A. P.; Burant, J. C.; Iyengar, S. S.; Tomasi, J.; Cossi, M.; Rega, N.; Millam, N. J.; Klene, M.; Knox, J. E.; Cross, J. B.; Bakken, V.; Adamo, C.; Jaramillo, J.; Gomperts, R.; Stratmann, R. E.; Yazyev, O.; Austin, A. J.; Cammi, R.; Pomelli, C.; Ochterski, J. W.; Martin, R. L.; Morokuma, K.; Zakrzewski, V. G.; Voth, G. A.; Salvador, P.; Dannenberg, J. J.; Dapprich, S.; Daniels, A. D.; Farkas, Ö.; Foresman, J. B.; Ortiz, J. V.; Cioslowski, J.; Fox, D. J. *Gaussian 09*, Gaussian, Inc.: Wallingford, CT, USA, 2009.
48. Jayatilaka, D.; Grimwood, D. J., Tonto: A Fortran Based Object-Oriented System for Quantum Chemistry and Crystallography. In *Computational Science — ICCS 2003*, Sloot, P. M. A.; Abramson, D.; Bogdanov, A. V.; Dongarra, J. J.; Zomaya, A. Y.; Gorbachev, Y. E., Eds. Springer-Verlag: 2003; pp 142-151.
49. Allen, F. H.; Bruno, I. J., Bond lengths in organic and metal-organic compounds revisited: X-H bond lengths from neutron diffraction data. *Acta Crystallogr B* **2010,** *66*, 380-386.
50. Neese, F., The ORCA Program System. *WIREs Comput. Molec. Sci.* **2012,** *2*, 73-78.
51. Neese, F., Software update: the ORCA program system, version 4.0. *Wires Comput Mol Sci* **2018,** *8* (1), e1327.

52. Becke, A. D., Density Functional Calculations of Molecular Bond Energies. *J. Chem. Phys.* **1988,** *84*, 4524.
53. Perdew, J. P., Density-Functional Approximation for the Correlation Energy of the Inhomogeneous Electron Gas. *Phys. Rev. B* **1986,** *33*, 8822.
54. Barone, V.; Cossi, M., Quantum Calculation of Molecular Energies and Energy Gradients in Solution by a Conductor Solvent Model. *J. Phys. Chem. A* **1998,** *102*, 1995.
55. Schäfer, A.; Horn, H.; Ahlrichs, R., Fully Optimized Contracted Gaussian Basis Sets for Atoms Li to Kr *J. Chem. Phys.* **1992,** *97*, 2571-2577.
56. Schäfer, A.; Huber, C.; Ahlrichs, R., Fully Optimized Contracted Gaussian Basis Sets of Triple Zeta Valence Quality for Atoms Li to Kr *J. Chem. Phys.* **1994,** *100*, 5829-5835.
57. Weigend, F.; Ahlrichs, R., Balanced Basis Sets of Split Valence, Triple Zeta Valence and Quadrupole Zeta Valence Quality for H to Rn: Design and Assessment of Accuracy. *Phys. Chem. Chem. Phys.* **2005,** *7*, 3297.
58. Grimme, S.; Antony, J.; Ehrlich, S.; Krieg, H., A Consistent and Accurate ab initio Parametrization of Density Functional Dispersion Correction (DFT-D) for the 94 Elements H-Pu. *J. Chem. Phys.* **2010,** *132*, 154104.
59. Grimme, S.; Ehrlich, S.; Goerigk, L., Effect of the Famping Function in Dispersion Corrected Density Functional Theory. *J. Comput. Chem.* **2011,** *32*, 1456.
60. van Lenthe, E.; Snijders, J. G.; Baerends, E. J., The Zero–Order Regular Approximation for Relativistic Effects: The Effect of Spin–Orbit Coupling in Closed Shell Molecules. *J. Chem. Phys.* **1996,** *105*, 6505.
61. van Lenthe, E.; van der Avoird, A.; Wormer, P. E. S., Density Functional Calculations of Molecular Hyperfine Interactions in the Zero Order Regular Approximation for Relativistic Effects. *J. Chem. Phys.* **1998,** *108*, 4783.
62. van Lenthe, J. H.; Faas, S.; Snijders, J. G., Gradients in the ab initio Scalar Zeroth-Order Regular Approximation (ZORA) Approach. *Chem. Phys. Lett.* **2000,** *328*, 107.
63. van Wüllen, C. J., Molecular Density Functional Calculations in the Regular Relativistic Approximation: Method, Application to Coinage Metal Diatomics, Hydrides, Fluorides and Chlorides, and Comparison with First-Order Relativistic Calculations. *J. Chem. Phys.* **1998,** *109*, 392.
64. Neese, F., An Improvement of the Resolution of the Identity Approximation for the Formation of the Coulomb Matrix. *J. Comput. Chem.* **2003,** *24*, 1740.
65. Roos, B. O.; Taylor, P. R.; Siegbahn, P. E. M., A Complete Active Space SCF Method (CASSCF) Using a Density-Matrix Formulated Super-CI Approach. *Chem. Phys.* **1980,** *48*, 157.
66. Siegbahn, P. E. M.; Heiberg, A.; Roos, B.; Levy, B., A Comparison of the Super-CI and the Newton-Raphson Scheme in the Complete Active Space SCF Method. *Phys. Scr.* **1980,** *21*, 323.
67. Siegbahn, P. E. M.; Almlof, J.; Heiberg, A.; Roos, B. O., The Complete Active Space SCF (CASSCF) Method in a Newton-Raphson Formulation with Application to the HNO Molecule. *J. Chem. Phys.* **1981,** *74*, 2384.
68. Angeli, C.; Cimiraglia, R.; Evangelisti, S.; Leininger, T.; Malrieu, J.-P., Introduction of *N*-Electron Valence States for Multireference Perturbation Theory. *J. Chem. Phys.* **2001,** *114*, 10252.
69. Angeli, C.; Cimiraglia, R.; Malrieu, J.-P., *N*-Electron Valence State Perturbation Theory: A Fast Implementation of the Strongly Contracted Variant. *Chem. Phys. Lett.* **2001,** *350*, 297-305.

70. Angeli, C.; Cimiraglia, R., *N*-Electron Valence State Perturbation Theory: A Spinless Formulation and an Efficient Implementation of the Strongly Contracted and of the Partially Contracted Variants. *J. Chem. Phys.* **2002,** *117*, 9138.
71. Angeli, C.; Cimiraglia, R., Multireference Perturbation Configuration Interaction V. Third-Order Energy Contributions in the Møller-Plesset and Epstein-Nesbet Partitions. *Theor. Chem. Acc.* **2002,** *107*, 313.
72. Ganyushin, D.; Neese, F., A Fully Variational Spin-Orbit Coupled Complete Active Space Self-Consistent Field Approach: Application to Electron Paramagnetic Resonance g-Tensors. *J. Chem. Phys.* **2013,** *138*, 104113.
73. Vallet, V.; Maron, L.; Teichteil, C.; Flament, J.-P., A Two-Step Uncontracted Determinantal Effective Hamiltonian-Based SO-CI Method. *J. Chem. Phys.* **2000,** *113*, 1391.
74. Maurice, R.; Bastardis, R.; Graaf, C. d.; Suaud, N.; Mallah, T.; Guihéry, N., Universal Theoretical Approach to Extract Anisotropic Spin Hamiltonians. *J. Chem. Theory Comput.* **2009,** *5*, 2977.
75. Jung, J.; Atanasov, M.; Neese, F., Ab Initio Ligand-Field Theory Analysis and Covalency Trends in Actinide and Lanthanide Free Ions and Octahedral Complexes. *Inorg. Chem.* **2017,** *56*, 8802-8816.
76. Singh, S. K.; Eng, J.; Atanasov, M.; Neese, F., Covalency and Chemical Bonding in Transition Metal Complexes: An ab initio Based Ligand Field Perspective. *Coord. Chem. Rev.* **2017,** *344*, 2-25.
77. Trzhtsinskaya, B. V.; Abramova, N. D., Imidazole-2-Thoines: Synthesis, Structure, Properties. *Sulfur Reports* **1991,** *10*, 389.
78. Prananto, Y. P.; Turner, D. R.; Duriska, M. B.; Lu, J.; Batten, S. R., Three-Centre, Two-Electron Bonds in Complexes of Mn, Ni, Co and Cd with 3-(4-benzonitrile)pyrazolyl Scorpionates. *Inorg. Chim. Acta* **2009,** *362*, 4646.
79. Ruman, T.; Ciunik, Z.; Goclan, A.; Łakasiewicz, M.; Wołowiec, S., Complexes of Heteroscorpionate Trispyrazolylborate Anionic Ligands. Part V. X-ray Crystallographic Studies of Cobalt(II) Complexes with Hydrobis(3,5-dimethylpyrazolyl)(3,5-diphenylpyrazolyl)borate and Hydrobis(3,5-diphenylpyrazolyl)(3,5-dimethylpyrazolyl)borate Ligands. *Polyhedron* **2001,** *20*, 2965.
80. Wang, Y.-L.; Cao, R.; Bi, W.-H., Syntheses and Characterizations of Co(II) and Ni(II) Complexes of Dihydrobis(thioxotetrazolyl)borato with Co[S_4] and Ni[S_4H_2] Cores. *Polyhedron* **2005,** *24*, 585.
81. Ghosh, P.; Bonanno, J. B.; Parkin, G., Synthesis and Structure of [$Bp^{tBu,iPr}$]$_2$Co: A Bis(pyrazolyl)hydroborato Cobalt(II) Complex with *trans* [Co···H–B] Interactions. *J. Chem. Soc., Dalton Trans.* **1998**, 2779.
82. Pinsky, M.; Avnir, D., Continuous symmetry measures. 5. The classical polyhedra. *Inorganic Chemistry* **1998,** *37* (21), 5575-5582.
83. Cotton, F. A.; Goodgame, D. M. L.; Goodgame, M., The Electronic Structures of Tetrahedral Cobalt(II) Complexes. *J. Am. Chem. Soc.* **1961,** *83*, 4690.
84. Banci, L.; Bencini, A.; Benelli, C.; Gatteschi, D.; Zanchini, C., Spectral-Structural Correlations in High-Spin Cobalt(II) Complexes. *Struct. Bond.* **2007,** *52*, 37.
85. Korchagin, D. V.; Palii, A. V.; Yureva, E. A.; Akimov, A. V.; Misochko, E. Y.; Shilov, G. V.; Talantsev, A. D.; Morgunov, R. B.; Shakin, A. A.; Aldoshin, S. M.; Tsukerblat, B. S., Evidence of field induced slow magnetic relaxation in cis-[Co(hfac)2(H2O)2] exhibiting

tri-axial anisotropy with a negative axial component. *Dalton Transactions* **2017,** *46* (23), 7540-7548.
86. Palii, A. V.; Korchagin, D. V.; Yureva, E. A.; Akimov, A. V.; Misochko, E. Y.; Shilov, G. V.; Talantsev, A. D.; Morgunov, R. B.; Aldoshin, S. M.; Tsukerblat, B. S., Single-Ion Magnet Et4N[CoII(hfac)3] with Nonuniaxial Anisotropy: Synthesis, Experimental Characterization, and Theoretical Modeling. *Inorganic Chemistry* **2016,** *55* (19), 9696-9706.
87. Gatteschi, D.; Sessoli, R.; Villain, J., *Molecular nanomagnets*. Oxford University Press: Oxford ; New York, 2006; p xii, 395 p.
88. Abragam, A.; Bleaney, B., *Electron paramagnetic resonance of transition ions*. Clarendon P.: Oxford, 1970; p xiv, 911 p.
89. Zein, S.; Duboc, C.; Lubitz, W.; Neese, F., A Systematic Density Functional Study of the Zero-Field Splitting in Mn(II) Coordination Compounds. *Inorganic Chemistry* **2008,** *47* (1), 134-142.
90. Gomez-Coca, S.; Cremades, E.; Aliaga-Alcalde, N.; Ruiz, E., Mononuclear Single-Molecule Magnets: Tailoring the Magnetic Anisotropy of First-Row Transition-Metal Complexes. *J Am Chem Soc* **2013,** *135* (18), 7010-7018.
91. Ruamps, R.; Batchelor, L. J.; Maurice, R.; Gogoi, N.; Jiménez-Lozano, P.; Guihéry, N.; de Graaf, C.; Barra, A.-L.; Sutter , J.-P.; Mallah, T., Origin of the Magnetic Anisotropy in Heptacoordinate NiII and CoII Complexes. *Chemistry – A European Journal* **2013,** *19* (3), 950-956.
92. Charron, G.; Malkin, E.; Rogez, G.; Batchelor, L. J.; Mazerat, S.; Guillot, R.; Guihery, N.; Barra, A. L.; Mallah, T.; Bolvin, H., Unraveling sigma and pi Effects on Magnetic Anisotropy in cis-NiA(4)B(2) Complexes: Magnetization, HF-HFEPR Studies, First-Principles Calculations, and Orbital Modeling. *Chem-Eur J* **2016,** *22* (47), 16848-16860.
93. Holladay, A.; Leung, P.; Coppens, P., Generalized Relations between D-Orbital Occupancies of Transition-Metal Atoms and Electron-Density Multipole Population Parameters from X-Ray-Diffraction Data. *Acta Cryst.* **1983,** *A39*, 377.
94. Damgaard-Møller, E.; Krause, L.; Tolborg, K.; Macetti, G.; Genoni, A.; Overgaard, J., Quantification of the Magnetic Anisotropy of a Single-Molecule Magnet from the Experimental Electron Density. *Angewandte Chemie International Edition* **2020**.
95. Bader, R. F. W., *Atoms in Molecules : A Quantum Theory*. Claredon Press: Oxford, 1990.
96. Gatti, C., Chemical bonding in crystals: new directions. *Zeitschrift Fur Kristallographie* **2005,** *220* (5-6), 399-457.
97. Vaidya, S.; Upadhyay, A.; Singh, S. K.; Gupta, T.; Tewary, S.; Langley, S. K.; Walsh, J. P. S.; Murray, K. S.; Rajaraman, G.; Shanmugam, M., A synthetic strategy for switching the single ion anisotropy in tetrahedral Co(II) complexes. *Chem Commun* **2015,** *51* (18), 3739-3742.
98. Gupta, T.; Rajaraman, G., Modelling spin Hamiltonian parameters of molecular nanomagnets. *Chem Commun* **2016,** *52* (58), 8972-9008.
99. Craig, G. A.; Sarkar, A.; Woodall, C. H.; Hay, M. A.; Marriott, K. E. R.; Kamenev, K. V.; Moggach, S. A.; Brechin, E. K.; Parsons, S.; Rajaraman, G.; Murrie, M., Probing the origin of the giant magnetic anisotropy in trigonal bipyramidal Ni(II) under high pressure. *Chem Sci* **2018,** *9* (6), 1551-1559.

For Table of Contents Only

TOC graphic

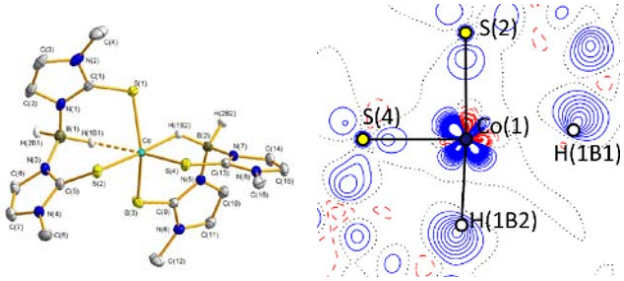

Synopsis.

Herein, we use ab initio calculations, electronic spectroscopy and experimental charge density studies to study the electronic structure and magnetic properties of a six-coordinate Co(II) complex. We illustrate the importance of the often-neglected value of transverse anisotropy, E, and advocate an adjustment to the over-simplified dichotomous easy-axis/easy-plane nomenclature often found in the literature. Finally, we derive experimental d-orbital populations that match quantitatively theoretical values, if bonding contributions from a MO analysis are taken into account.